Optimization of empirical beamhardening correction algorithm

Andriy Andreyev*[a], Faguo Yang[a], Lars Omlor[a], Matthew Andrew[a]
[a] Carl Zeiss X-ray Microscopy, Inc, 5300 Central Parkway, Dublin, CA, USA 94568

ABSTRACT

Metal artifacts are one of the most common reasons for reduced image quality and usability in polychromatic cone-beam CT. In this work, we revisit empirical beam hardening correction algorithm and propose a few practical optimizations to simplify its application. First, fuzzy C-means segmentation method is used to perform an automatic segmentation of the metal component. Second, a minimum variance optimization technique provides a suitable combination of correction basis images. Finally, a sub-volume (spatially varying) optimization method is used to account for a varying contribution of metal artifacts through the image. We apply the modified algorithm to datasets from cone-beam CT and evaluate its performance.

Keywords: Cone beam CT, image reconstruction, metal artifact reduction, beamhardening, fuzzy C-means.

1. INTRODUCTION

Metal artifacts are one of the primary causes for image quality degradation in Computed Tomography. The streaks and shadows caused by the artifacts obscure the useful information content, prevent robust segmentation and feature detection in medical as well as industrial CT imaging. Numerous algorithmic methods have been proposed over the years to resolve the problem of metal artifact reduction (MAR). These include but not limited to segmentation-based [1, 3, 5], inpainting or projection completion based [6], iterative model-based [3],[7], machine-learning based [8], and so on. More comprehensive overview of various metal artifact correction can be found in [9].

In this work we revisit an empirical beam hardening correction method (EBHC) [1] and propose a few practical modifications and enhancements, in order to reduce its reliance on manual user intervention. We apply the modified method to a number of cases from CBCT and discuss the results.

2. METHODS

The polychromatic nature of most X-ray sources used in CT leads to artifacts in the reconstructed images. These are most evident whenever studied objects and samples demonstrate high variability in atomic number (Z). The artifacts take the form of dark streaks and halos as shown in Figure 1.

While it is possible to minimize the severity of metal artifacts by modifying the acquisition conditions, the most common artifact correction solutions are algorithmic. Here, we try to build upon and add a few modifications to an empirical beam hardening correction method which has proven its effectiveness despite its relative simplicity [1]. The primary goal of the proposed modifications is to make the EBHC application more autonomous, without requiring user intervention.

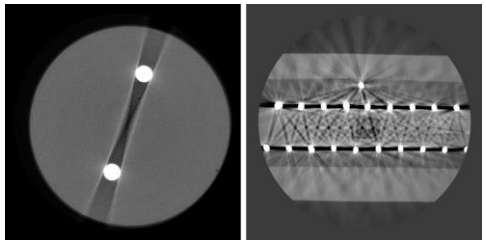

(a) (b)

Figure 1. Examples of samples in CBCT that lead to creation of metal artifacts: a) cylindrical phantom with plastic filling and two 4mm diameter brass rod inserts. b) HDMI connector.

*andriy.andreyev@zeiss.com; www.zeiss.com/microscopy

7th International Conference on Image Formation in X-Ray Computed Tomography,
edited by Joseph Webster Stayman, Proc. of SPIE Vol. 12304, 1230433
 · 0277-786X · doi: 10.1117/12.2647155

EBHC consists of the following steps:

1. The acquired dataset g is being reconstructed to create 3D tomographic image as $f = F^{-1}g$, where F^{-1} is the tomographic reconstruction algorithm of choice; no metal artifact related correction is necessary at this stage, however, in many cases simple polynomial based beam hardening correction may reduce cupping artifacts and enhance the image structures which will help with the next step.

2. The reconstructed CT image f is segmented to extract only the metal component m.

3. Results of the segmentation is then forward projected in the matching geometry to the original acquisition. Forward projection can be done in monochromatic fashion, however it is important that it follows the geometry as close as possible.

$$h^j = Fm$$

4. The forward projected data h is then combined with the original data g to create a set of basis data p_{ij}:

$$p_{ij} = g^i h^j,$$

where i and j can be lower integer values ranging from 0 to 5 as an example. Not all possible combinations of i and j need to be considered due to increased computational burden and somewhat overlapping nature of these correction terms.

5. Each data combination p_{ij} is then reconstructed using reconstruction operation F^{-1} to create corresponding set of images f_{ij}. We further denote uncorrected reconstructed image as f_{10}.

6. The higher order basis images that include forward projected metal component are effectively able to replicate the metal artifact streaks. As such, the generated set of basis images can be combined using a certain optimal set of weighting coefficients to create a final corrected image that can effectively mitigate the effect of metal artifacts. In this work, original uncorrected image always uses the weight of 1.0, and the rest of the images can have variable weighting coefficients (negative values are also possible). This workflow is shown in figure 2.

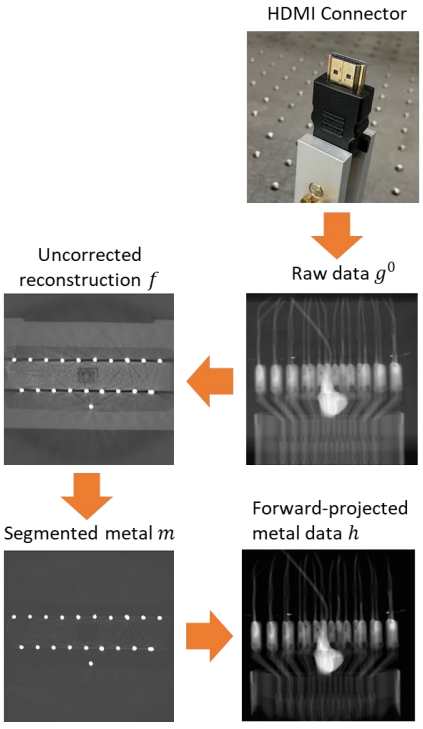

Figure 2. Diagram of the EBHC method, describing the first part of the method, leading to the forward projected data generation.

In original EBHC method soft thresholding was used to segment out the high-density components. In this work we found that fuzzy C-means segmentation can be very effective method as implemented in [10]. We used two material segmentation with starting values for the low-Z material segmentation set at zero, and high-Z material set at 80% of the maximum value of f. To improve robustness of the segmentation it is also advisable to prefilter the image before the segmentation with edge preserving filter, such as median filter.

The basis functions are combined according to the following equation:

$$\hat{f} = \begin{cases} f_{10} & m > 1 \\ f_{10} + \sum_{i,j} w_{ij} f_{ij} & m = 0 \end{cases}$$

In this way no correction has been applied inside the metal parts, as we seek to mitigate the streak artifacts in between metal/higher-Z components.

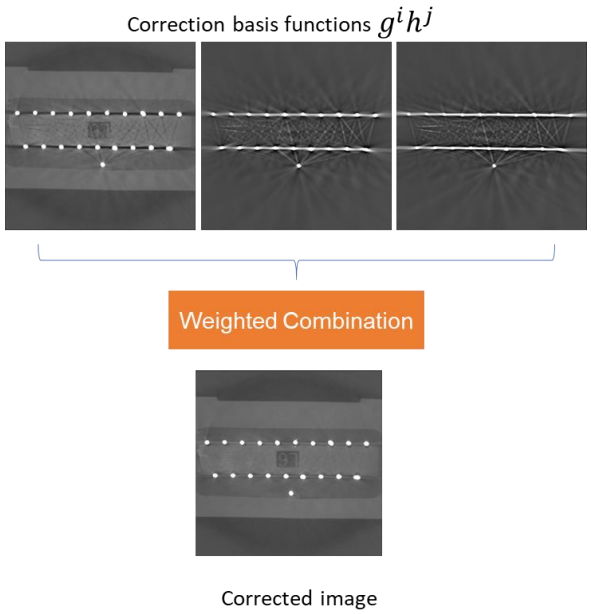

Figure 3. Second part of the EBHC method: optimal weighted sum of basis images leads to a reduction in metal artifact expression.

Optimal weight determination is then the significant outstanding challenge. One obvious way is to do this manually, ad hoc going through all possible combinations of w_{ij} that can provide artifact streak reduction while maintaining the image quality. The success of such method may vary and depends on the operator training. Additionally, any manual, operator-controlled optimization method is tedious to perform with more than two or three basis images, and any optimization is global, with a single set of weights determined for the entire image (in contrast to an automated technique which may be allowed to vary spatially).

In some cases, to simplify the optimization process, it may also be feasible to define the region in the reconstructed image that is known to be flat but has been imbued with spurious signal from the artifact streaks. Some examples of such flat region include uniform plastic enclosure surrounding the metal wires, or soft tissue surrounding metal implants or bone matter for biological samples. The assumption is that proper combination of basis images will minimize the streaks and will make such region more uniform. In this work, we propose to use minimum variance-based optimizer, estimated over the entire volume excluding metal/high-Z components. This also means that entire EBHC workflow can now be performed fully automatically (referred to in the text as automatic EBHC (AEBHC)). The further advantage of such automatic optimization method is that it can take arbitrary number of basis functions as an input without any complication for the user (other than prolonged reconstruction time).

As the objects can be highly non-uniform, with different amount of beamhardening, scatter, and metal artifact presence in each slice, a globally optimized single set of combination weights may result in under- or overcorrection of certain sub-volumes (slices). Likewise, it is not practically feasible to have those hand-tuned for each sub-volume, as it would be a very tedious task. We propose that optimization weights are recalculated for every sub-volume in AEBHC. Here we recalculate the weight every 64 slices, while averaging the individually optimized sub-volumes into the final volume using 50% overlap.

Overall, all the discussed modifications allow for a high degree of EBHC autonomy, allowing single-click metal artifact reductions.

3. RESULTS AND DISCUSSIONS

To provide some examples of the reconstruction, use tomographic 3D X-ray microscopy data from Zeiss Xradia Versa (Carl Zeiss X-Ray Microscopy, Dublin, CA).

The first example is the cylindrical phantom from Figure 1. Correction with AEBHC was able to drastically reduce the severity of the metal artifacts and the visual conspicuity of a small void indicated was much improved as shown in Figure 4.

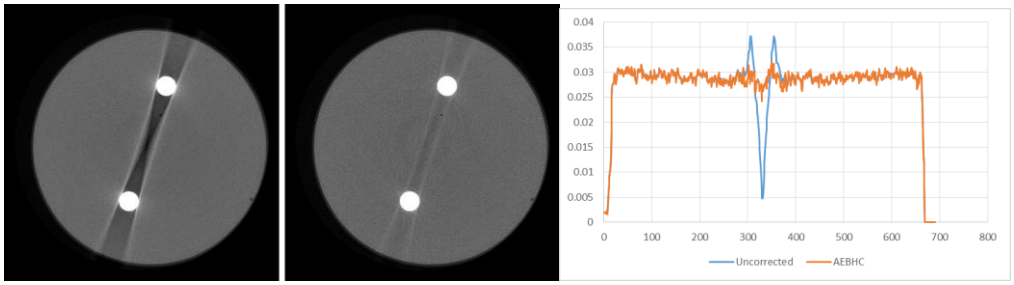

(a) (b) (c)

Figure 4. Cylindrical phantom with plastic filling and two 4mm diameter brass rod inserts: a) uncorrected FDK reconstruction; b) corrected with AEBHC; c) reconstructed intensity profiles, drawn across the phantom from approximately 10 to 4 o'clock.

Three scans of a standard HDMI connector have been performed to test the performance of auto-EBHC method at different acquisition conditions. Acquisition conditions included 160 and 100 kVp, as well as stronger (equivalent to approximated 2 mm of Cu) and medium filter. In Figure 5, we show both uncorrected and AEBHC corrected images. From the images it is clear that higher kVp and stronger filtered X-ray spectrum (removing lower energy part of the spectrum) helps to reduce the severity of metal artifacts even in the uncorrected data. The artifacts are more severe at lower kVp, showing that acquisition parameters play a strong role in AEBHC effectiveness. AEBHC performs better at higher X-ray energy setting, and stronger filter (first column, Figure 5), however, corrected reconstructions outperform uncorrected reconstructions at all conditions.

The advantage of sub-volume optimized AEBHC method is demonstrated in Figure 6. Here, we use simple phantom consisting of steel rods, plastic tubes inserted into the piece of plastic foam. In Figure 6 we show two reconstructed slices through the phantom, with both AEBHC and manually optimized EBHC method. Manual optimization of weights for EBHC was done over the slice shown in the top, and then applied globally to the entire volume. That leads to overcorrection for metal artifacts in the slice 200 shown in the bottom row. AEBHC was able to perform more consistently avoiding overcorrection across the entire volume.

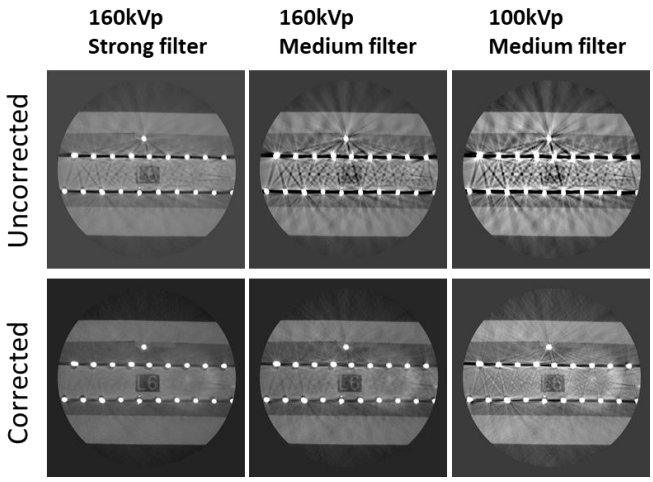

Figure 5. Reconstructions of HDMI cable connector, performed at different 160 and 100 kVp, as well as with stronger (~2mm Cu thickness) and medium (1mm Cu thickness) filtering material. Uncorrected and corrected reconstructions are in top and bottom row respectively.

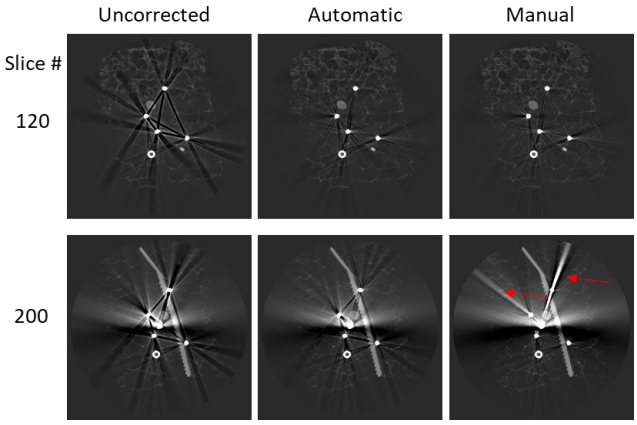

Figure 6. Reconstructions of simple steel rods phantom. Manual optimization of global weighting correction parameters was performed for the slice 120.

4. CONCLUSION

We have demonstrated an improvement an empirical beam hardening correction method, combining three techniques to make the EBHC method fully automatic, with a good approximation for metal artifacts. First, fuzzy C-means was used to perform an automatic segmentation of the metal component. Second, a minimum variance optimization method was used to provide a suitable combination of correction basis functions. Finally, a sub-volume (spatially varying) optimization method was used to account for a varying contribution of metal artefacts through the image. The proposed method has been tested across the variety of samples and acquisition conditions and was able to noticeably diminish the severity of metal artifacts. It was also able to perform similarly to manually optimized method, as well as outperform manual method globally. We also foresee that some of the proposed modifications can be applied to other variations of beamhardening correction algorithms.

ACKNOWLEDGEMENTS

The authors are grateful to Dr. Martin Krenkel and Dr. Daniel Weiss from Carl Zeiss Industrial Solutions (Oberkochen, Germany) for useful ideas and discussions.

REFERENCES

[1] Kyriakou, Y., Meyer, E., Prell, D., and Kachelrieß, M., “Empirical beam hardening correction (EBHC) for CT,” Medical Physics, 37, 5179 (2010).

[2] Van Gompel, G., Van Slambrouck, K., Defrise, M., Batenburg, K. J., de Mey, J., Sijbers, J., Nuyts, J., “Iterative correction of beam hardening artifacts in CT,” Med. Phys. 38, S36 (2011).

[3] Meyer, E., Raupach, R., Lell, M., Schmidt, B., Kachelrieß, M., “Frequency split metal artifact reduction (FSMAR) in computed tomography,” Med. Phys., 39(4), 1904-16 (2012).

[4] Zeng, G.L., Zeng, M., “Reducing metal artifacts by restricting negative pixels,” Vis Comput Ind Biomed Art., 4(1):17 (2021).

[5] Zeng, G.L., “A projection-domain iterative algorithm for metal artifact reduction by minimizing the total-variation norm and the negative-pixel energy,” Vis Comput Ind Biomed Art, Jan 2;5(1):1, 2022.

[6] Zhang, Y., Pu, Y.F., Hu, J.R., Liu, Y., Zhou, J.L., “A new CT metal artifacts reduction algorithm based on fractional-order sinogram inpainting,” J X-Ray Sci Technol.;19(3):373–384 (2011).

[7] Stayman, J.W., Otake, Y., Prince, J.L., Khanna, A.J., and Siewerdsen, J.H., ‘‘Model-based tomographic reconstruction of objects containing known components,’’ IEEE Trans. Med. Imag., vol. 31, no. 10, pp. 1837–1848 (2012).

[8] Xu, S., Dang, H., “Deep residual learning enabled metal artifact reduction in CT,” Proc. SPIE 10573, Medical Imaging (2018).

[9] Gjesteby, L., De Man, B., Jin, Y., Paganetti, H., Verburg, J., Giantsoudi, D., Wang, G., "Metal Artifact Reduction in CT: Where Are We After Four Decades?," in IEEE Access, vol. 4, pp. 5826-5849 (2016).

[10] Ahmed, M. N., Yamany, S.M., Mohamed, N., Farag, A.A. and Moriarty, T., "A modified fuzzy c-means algorithm for bias field estimation and segmentation of MRI data," in IEEE Transactions on Medical Imaging, vol. 21, no. 3, pp. 193-199 (2002).